Design and Optimization of a Photon Counting Detection Apparatus for Geontropic Fluctuations in Spacetime

Rafael Crespo

California Institute of Technology

September 27, 2024

Abstract

The pursuit of detecting geontropic fluctuations in the metric of spacetime has led to the development of an advanced photon counting apparatus designed to enhance sensitivity and distinguish the desired signals from background noise. The new apparatus in the RbQ experiment leverages an atomic cavity, incorporating a laser-cooled cloud of Rubidium atoms within a 4-mirror setup. This configuration, featuring two curved mirrors and two flat mirrors, aims to minimize signal loss and optimize the filtering effect of incoming photons. By modeling various cavity designs using Finesse-3 on Python, the beam profile was refined to achieve a minimized waist, which is crucial for increasing the probability of photon-atom interactions. The simulation revealed that adjusting the angle of the curved mirrors effectively reduced the beam size, with an optimal minimum angle of $3.20°$ determined to avoid clipping. This work on the starting design of RbQ contributes to enhancing detection sensitivity for quantum gravity research and lays the groundwork for potential exploration of more complex cavity geometries in the future.

Contents

1 Introduction

This report details the design of an advanced optical cavity based on a photon counting technique aimed at improving the detection of weak signals, including the predicted geontropic fluctuations in spacetime metrics from quantum gravity theories. The apparatus employs an atomic cavity with laser-cooled Rubidium atoms to enhance sensitivity by distinguishing the desired signal from other noise sources. The optical setup (Figure 1) features a 4-mirror arrangement where two mirrors are curved to focus the incoming laser beam to its smallest waist, increasing the probability of photon interaction with the Rb atoms. This design reduces signal loss and enhances the filtering of incoming light. The detection method involves measuring the state of the valence electron in the Rb atom after interaction with the output signal from the interferometer (IFO). If the valence electron is in an excited state, it indicates successful absorption of the signal photon, confirming the detection of the desired signal. In reality, the actual readout scheme is more complex; however, a comprehensive description is beyond the scope of this report. [1].

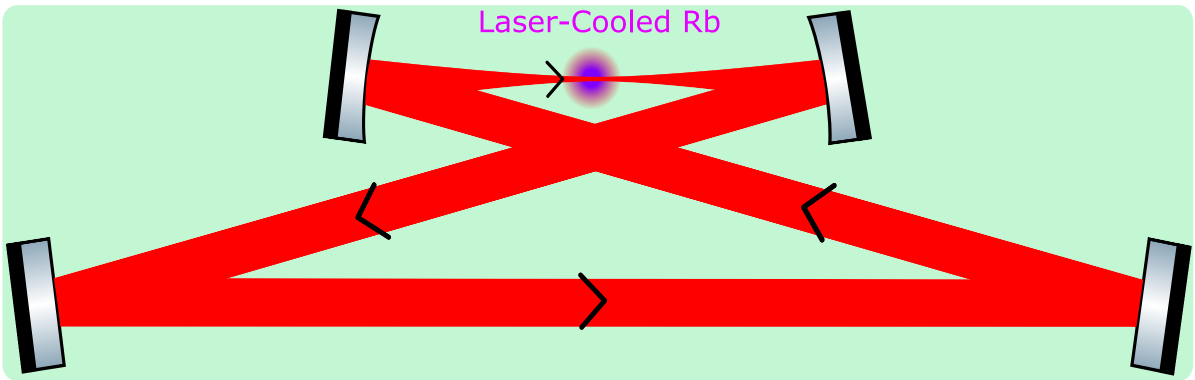

Figure 1: Diagram of 4-mirror laser cavity. Mirrors are numbered following the beam's trajectory, starting at the top-left (Top-left: M1, Top-Right: M2, Bottom-Left: M3, and Bottom-Right: M4. Cloud of laser-cooled Rb atoms are located at the waist between M1 and M2.

2 Design Process

To design the 4-mirror cavity, Finesse 3 was employed to simulate the laser cavity and model the beam profile with varying lengths and angles. This simulation calculates critical beam characteristics such as beam waist (w_0), beam size (w), and Rayleigh range (z_R), among others, by parameterizing the distance between mirrors, angle of incidence (AOI), and the radius of curvature (RoC) of the mirrors. The goal was to identify the configuration that minimizes the beam size at the waist, as illustrated in Figure 2.

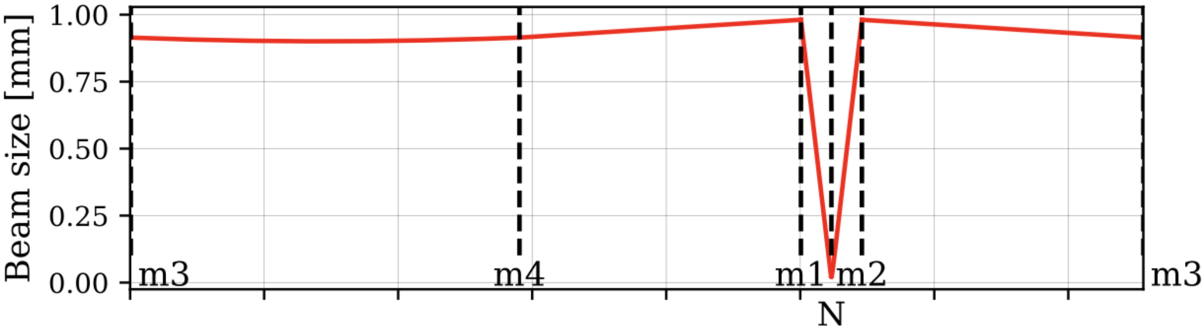

Figure 2: Plot of Beam Size along beam path. AOI = $3.2°$, $L_1 = 0.091$m, $L_2 = 0.42$m, $L_3 = 0.58$m, $L_4 = 0.42$m.

2.1 Determining Impact of Different Path Lengths on Beam Size.

With the goal of decreasing the beam size at the beam's waist between mirrors M1 and M2, I started out by trying different configurations of the 4 lengths between the mirrors. However, it was evident that just a small set of them were possible since most of the varying length configurations resulted in an unstable cavity, which was not desired. However, this sensitivity to the lengths was not equal among each of the lengths, and in particular, L_2, L_3, and L_4 could be changed much more than could L_1 before the cavity became unstable. Moreover, I found that the beam size, like the cavity's stability, was highly sensitive to changes in L_1 but less for the other lengths. Specifically, the beam size decreased greatly as L_1 got closer and closer to the RoC, while it did not change much as the other lengths were varied (see Figures 3 and 4).

These results are logical given that, for a fixed RoC, the Rayleigh length—defined as the distance from the beam waist along the optical axis at which the beam size reaches $\sqrt{2}$ times the waist size (see Appendix A)—is relatively large for the paths connecting M2 to M3, M3 to M4, and M4 to M1 (Table 3). Consequently, small changes in the other path lengths are insufficient compared to z_R to significantly affect the stability of the cavity or the waist size. Also of note, M3 and M4 are both flat mirrors, so their precise positions should not be too impactful on the cavity's stability and the waist size. On the other hand, L_1 being the length that connects the two curved mirrors naturally affects the waist between M1 and M2 the most. This prompted me to leave L_1 at about 1.01 times the RoC so as to produce a stable cavity while at the same time minimizing the waist size.

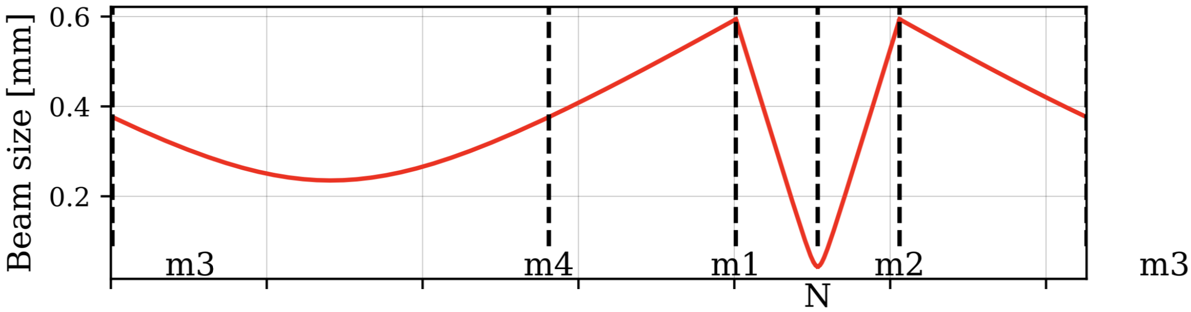

Figure 3: Plot of Beam Size along beam path with changed lengths. AOI = $3.2°$, $L_1 = 0.105$m, $L_2 = 0.12$m, $L_3 = 0.28$m, $L_4 = 0.12$m. This shows how a slight change in L_1 (about 0.014m or 15.4% increase from 0.091m) dramatically changed the beam size.

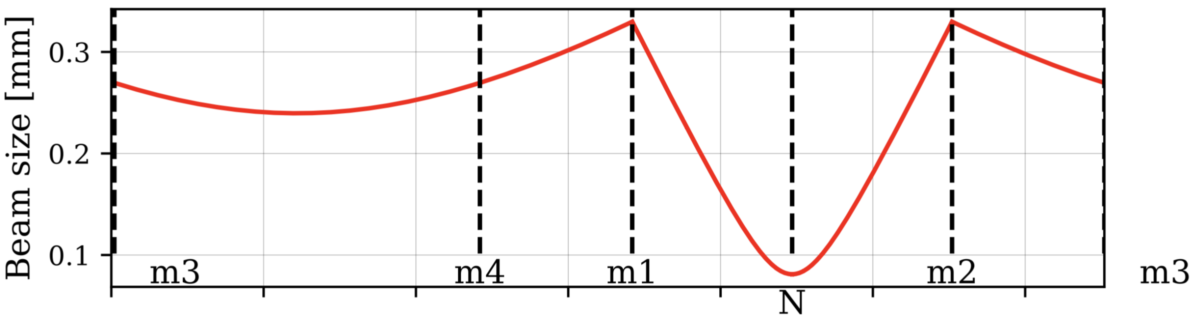

Figure 4: Plot of Beam Size along beam path with changed lengths. AOI = $3.2°$, $L_1 = 0.105$m, $L_2 = 0.12$m, $L_3 = 0.28$m, $L_4 = 0.12$m. This shows how a large relative change in the other lengths (about 58.3% decrease from 3) barely changed the beam size.

2.2 Testing Impact of RoC on Beam Size.

After seeing how L_1 had the greatest impact on the beam size given a fixed RoC, I set out to test the effect of different RoCs on the beam size since the radius of curvature of the mirrors determines the focusing effect on the beam. Here, it became evident that a lower RoC resulted in a lower beam size, which is fitting because a lower RoC means that the incoming beam is more greatly focused. This naturally leads to a smaller beam size at the waist.

Since the overall RbQ experiment involves other laser beams that need to go around the cavity, M1 and M2 could not be placed arbitrarily close. As a result, the RoC was set to 0.09m and L_1 was set to 0.091m (see Figure 2).

2.3 Clipping Angle Approximation Derivation

Along with the RoC and L_1, the angle of incidence (AOI) at M1 turned out to be highly impactful on the waist size of the beam. Specifically, after varying the AOI to determine that impact, I found that the waist monotonically decreased as the AOI decreased to 0°. This makes sense as a smaller AOI means the reflected beam carries a lower spread, resulting in a lower waist measurement. With that in mind, I had to find a limit to the AOI based upon the physical parameters. This limit was given by a need to prevent the beam from being physically blocked by the M1 and M2 mirrors. Concretely, this meant that the bottom of M1 should be at least 5σ away from the propagating beam's center. In this case, since the beam's intensity is given by $I(r,z) = I_0(\frac{w_0}{w(z)})^2 e^{-2\frac{r^2}{w^2(z)}}$, we have that $\sigma = \frac{w}{2}$. [2] In order to find this angle, I approximated the segment from the center of the beam to the bottom of M1 and that from the bottom of M1 to its center to be parallel (which was reasonable since the AOI would be small). In this approximation, the AOI could be determined with some trigonometry:

$$
\begin{aligned}
\tan\theta_i &= \frac{\Delta y}{L_1} \\
\theta_i &= \arctan\frac{\Delta y}{L_1} \\
&= \arctan\frac{20.2\text{ mm}}{180\text{ mm}} \\
&= 3.20^\circ.
\end{aligned}
\tag{1}
$$

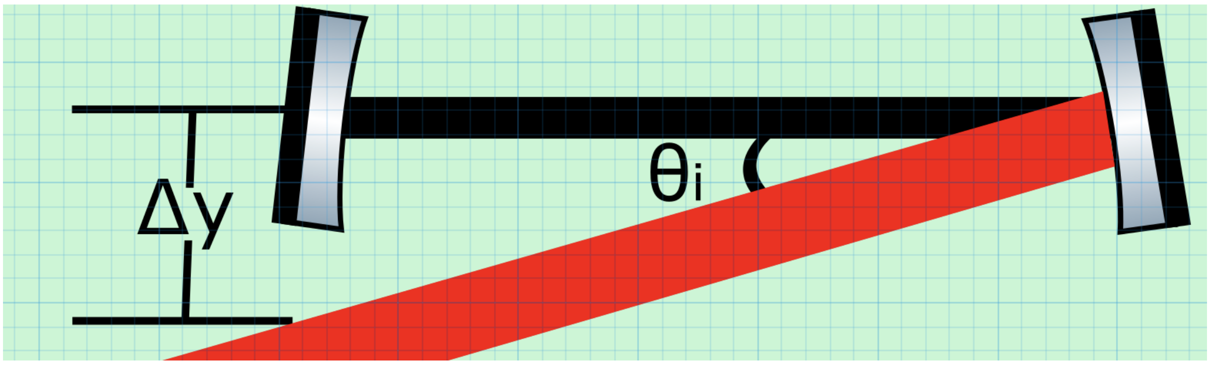

Figure 5: Diagram of AOI Approximation. In this derivation, Δy is the distance between the center of M1 and the closest point along the center of the beam, i.e. the sum of the 5σ segment and M1's radius: $\Delta y = 5\sigma + 0.5" = 5 * 1.5\text{ mm} + 12.7\text{ mm} = 20.2\text{ mm}$.

Note that this analysis determines the AOI of both M1 and M2 since the cavity was designed to be symmetrical between M1 and M2.

2.4 Checking Astigmatism of Cavity

With most of the cavity's parameters in place, it was important to make sure that the design had not introduced astigmatism, i.e., a difference in the waist size and location along the x-axis vs the y-axis. To do this, I used Finesse 3 to plot the beam size, along the cavity path, in the x-plane and separately the beam size in the y-plane (as can be seen in Figures 6 and 7).

Furthermore, I compared the parameter tables in the x-axis and y-axis, Table 1 and Table 2, respectively. There I noticed that the waist in the x-axis, 24.186µm, was higher than the waist in the y-axis, 22.891µm. However, this was a slight difference of 1.295µm or 5.657%.

Seeing that the beam size plots in Figures 6 and 7 have no noticeable difference, as well as the fact that Tables 1 and 2 show minimal discrepancies in their waist sizes, I decided

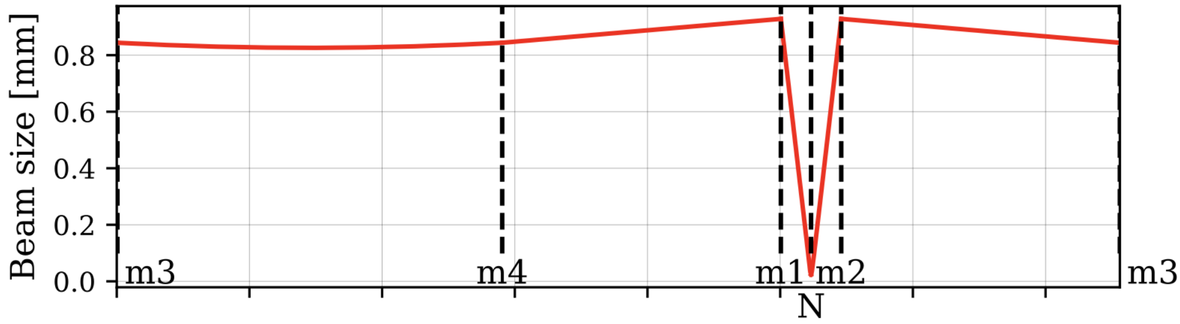

Figure 6: Plot of Beam Size along beam path in the x-plane.

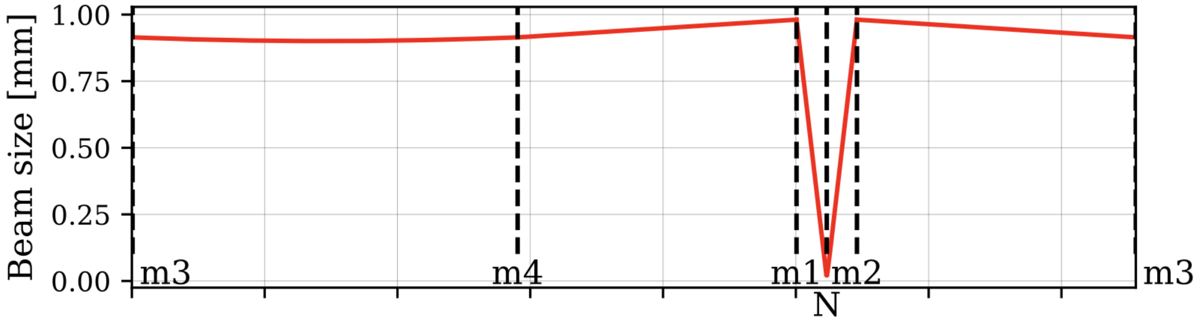

Figure 7: Plot of Beam Size along beam path in the y-plane.

Table 1: Table of beam properties at all optical elements along the beam trajectory in the x-plane.

	z	w0	zr	w	RoC	S	Acc. Gouy	q
L0.p1.o	0 m	825.98 um	1.3828 m	844.07 um	-6.8618 m	-145.73 mD	0°	-0.291 + 1.383j
m3.p1.i	1 mm	825.98 um	1.3828 m	843.95 um	-6.8834 m	-145.28 mD	39.684m°	-0.290 + 1.383j
m3.p3.o	1 mm	825.98 um	1.3828 m	843.95 um	-6.8834 m	-145.28 mD	39.684m°	-0.290 + 1.383j
m4.p1.i	581 mm	825.98 um	1.3828 m	843.95 um	6.8834 m	145.28 mD	23.729°	0.290 + 1.383j
m4.p2.o	581 mm	825.98 um	1.3828 m	843.95 um	6.8834 m	145.28 mD	23.729°	0.290 + 1.383j
m1.p4.i	1.001 m	825.98 um	1.3828 m	928.5 um	3.4031 m	293.85 mD	39.063°	0.710 + 1.383j
m1.p3.o	1.001 m	24.186 um	1.1856 mm	928.5 um	-45.531 mm	-21.963 D	39.063°	-0.045 + 0.001j
N.p1.i	1.0465 m	24.186 um	1.1856 mm	24.186 um	18.416 Gm	54.3 pD	127.57°	0.000 + 0.001j
N.p2.o	1.0465 m	24.186 um	1.1856 mm	24.186 um	18.416 Gm	54.3 pD	127.57°	0.000 + 0.001j
m2.p1.i	1.092 m	24.186 um	1.1856 mm	928.5 um	45.531 mm	21.963 D	216.08°	0.046 + 0.001j
m2.p2.o	1.092 m	825.98 um	1.3828 m	928.5 um	-3.4031 m	-293.85 mD	216.08°	-0.710 + 1.383j
m3.p4.i	1.512 m	825.98 um	1.3828 m	843.95 um	-6.8834 m	-145.28 mD	231.41°	-0.290 + 1.383j

Table 2: Table of beam properties at all optical elements along the beam trajectory in the y-plane.

	z	w0	zr	w	RoC	S	Acc. Gouy	q
L0.p1.o	0 m	900.52 um	1.6436 m	914.52 um	−9.5746 m	−104.44 mD	0°	−0.291 + 1.644j
m3.p1.i	1 mm	900.52 um	1.6436 m	914.43 um	−9.6056 m	−104.11 mD	33.803m°	−0.290 + 1.644j
m3.p3.o	1 mm	900.52 um	1.6436 m	914.43 um	−9.6056 m	−104.11 mD	33.803m°	−0.290 + 1.644j
m4.p1.i	581 mm	900.52 um	1.6436 m	914.43 um	9.6056 m	104.11 mD	20.046°	0.290 + 1.644j
m4.p2.o	581 mm	900.52 um	1.6436 m	914.43 um	9.6056 m	104.11 mD	20.046°	0.290 + 1.644j
m1.p4.i	1.001 m	900.52 um	1.6436 m	980.95 um	4.515 m	221.49 mD	33.403°	0.710 + 1.644j
m1.p3.o	1.001 m	22.891 um	1.0621 mm	980.95 um	−45.525 mm	−21.966 D	33.403°	−0.045 + 0.001j
N.p1.i	1.0465 m	22.891 um	1.0621 mm	22.891 um	81.28 Gm	12.303 pD	122.07°	0.000 + 0.001j
N.p2.o	1.0465 m	22.891 um	1.0621 mm	22.891 um	81.28 Gm	12.303 pD	122.07°	0.000 + 0.001j
m2.p1.i	1.092 m	22.891 um	1.0621 mm	980.95 um	45.525 mm	21.966 D	210.73°	0.046 + 0.001j
m2.p2.o	1.092 m	900.52 um	1.6436 m	980.95 um	−4.515 m	−221.49 mD	210.73°	−0.710 + 1.644j
m3.p4.i	1.512 m	900.52 um	1.6436 m	914.43 um	−9.6056 m	−104.11 mD	224.09°	−0.290 + 1.644j

to calculate the astigmatism directly using Finesse's built-in astigmatism detector as a final check. This produced an astigmatism (at the waist between M1 and M2) of 0.003021. Considering that the way Finesse 3 defines this property is such that a value of 1 means maximum astigmatism and a value of 0 means no astigmatism, this low calculated value indeed indicates that the cavity appears to have little astigmatism. This conclusion is also supported by the fact that the location of the waist is not different along the x-axis versus the y-axis. Nevertheless, more design work needs to be done in order to precisely determine if the calculated astigmatism for this particular experiment is low enough.

2.5 Consideration of Non-planar Design

While the design I had worked on was useful to understand the properties of the cavity necessary to minimize the beam waist, the light inside the cavity needs to be circularly polarized in order to interact properly with the ^{87}Rb atoms. Since planar cavities, which are those where the traveling light remains in a single plane, can only support one linear polarization at a time, the need for circular polarization required a non-planar cavity design. Unfortunately, Finesse 3 does not work well with non-planar cavity designs, so I had to consider ray transfer (ABCD) matrices. In planar optics, these are 2x2 matrices that transform a column vector that describes the incoming beam into a vector describing the outgoing beam:

$$\begin{bmatrix} x_2 \\ x_2^{'} \end{bmatrix} = \begin{bmatrix} A & B \\ C & D \end{bmatrix} \begin{bmatrix} x_1 \\ x_1^{'} \end{bmatrix} \tag{2}$$

In Equation 2, x_1 is the displacement of the incoming beam from the optical axis and $x_1^{'}$ is that beam's slope, while x_2 represents the displacement of the outgoing beam from the optical axis and $x_2^{'}$ is the outgoing beam's slope.

In the non-planar case, these matrices become 4x4 due to the additional y coordinate axis. [3]:

$$\left[\begin{array}{c} x_2 \\ x_2' \\ \hline y_2 \\ y_2' \end{array}\right] = \left[\begin{array}{cc|cc} A_{xx} & B_{xx} & A_{xy} & B_{xy} \\ C_{xx} & D_{xx} & C_{xy} & D_{xy} \\ \hline A_{yx} & B_{yx} & A_{yy} & B_{yy} \\ C_{yx} & D_{yx} & C_{yy} & D_{yy} \end{array}\right] \left[\begin{array}{c} x_1 \\ x_1' \\ \hline y_1 \\ y_1' \end{array}\right] \equiv \left[\begin{array}{c|c} M_{xx} & M_{xy} \\ \hline M_{yx} & M_{yy} \end{array}\right] \left[\begin{array}{c} x_1 \\ x_1' \\ \hline y_1 \\ y_1' \end{array}\right] \tag{3}$$

The on-diagonal matrices, M_{xx} and M_{yy} describe the impact of the incoming beam's x- and y-axis parameters with those of the outgoing beam along the same respective axes. The off-diagonal matrices, M_{xy} and M_{yx} account for the cross-axis effect when the beam bounces of the mirrors, thus relating how the incoming x-axis parameters change the outgoing y-axis parameters, and vice versa. In the non-planar cavity, these effects are caused by the off-planar rotations necessary to connect the 4 mirrors. In order to calculate the 4x4 matrix, I decided to focus first on M_{xx} and M_{yy}, the on-diagonal matrices. To do this, I determined the resulting matrix product, M, as if the four mirrors were co-planar because that is the source of the same-axis effects. In this computation, I utilized three standard ray transfer matrices:

1. **Free-space matrix** (FS): This matrix describes a ray traveling through space at a constant angle without interacting with any optical elements.

$$FS_i = \begin{bmatrix} 1 & L_i \\ 0 & 1 \end{bmatrix}$$

2. **Flat-mirror matrix** (M_3 and M_4): This matrix represents a ray perfectly reflecting off a flat mirror.

$$M_3 = M_4 = \begin{bmatrix} 1 & 0 \\ 0 & 1 \end{bmatrix}$$

3. **Curved-mirror matrix** (M_1 and M_2): This matrix models a ray reflecting off a spherical mirror with an effective radius of curvature R_e.

$$M_1 = M_2 = \begin{bmatrix} 1 & 0 \\ -\frac{2}{R_e} & 1 \end{bmatrix}$$

With these matrices in hand, I calculated the product by starting with the beam traveling in free space from M1 to M2 and ending with the beam bouncing off M1:

$$\begin{aligned} M &= M_1 \times FS_4 \times M_4 \times FS_3 \times M_3 \times FS_2 \times M_2 \times FS_1 \\ &= M_1 \times \begin{bmatrix} 1 & L_{2,3,4} \\ 0 & 1 \end{bmatrix} \times M_2 \times FS_1 \\ &= \begin{bmatrix} 1 & 0 \\ -\frac{2}{R_e} & 1 \end{bmatrix} \times \begin{bmatrix} 1 & L_{2,3,4} \\ 0 & 1 \end{bmatrix} \times \begin{bmatrix} 1 & 0 \\ -\frac{2}{R_e} & 1 \end{bmatrix} \times \begin{bmatrix} 1 & L_1 \\ 0 & 1 \end{bmatrix} \\ &= \begin{bmatrix} 1 & L_{2,3,4} \\ -\frac{2}{R_e} & 1 - \frac{2}{R_e} L_{2,3,4} \end{bmatrix} \times \begin{bmatrix} 1 & L_1 \\ -\frac{2}{R_e} & 1 - 2\frac{L_1}{R_e} \end{bmatrix} \\ &= \begin{bmatrix} 1 - \frac{2}{R_e} L_{2,3,4} & L_1 + (1 - 2\frac{L_1}{R_e}) L_{2,3,4} \\ \frac{4}{R_e^2}(L_{2,3,4} - R_e) & \frac{2}{R_e^2}(2L_1 - R_e)(L_{2,3,4} - R_e) - 1 \end{bmatrix} \\ &= \begin{bmatrix} 1 - \frac{2}{R\cos\theta_i} L_{2,3,4} & L_1 + (1 - 2\frac{L_1}{R\cos\theta_i}) L_{2,3,4} \\ \frac{4}{R^2\cos^2\theta_i}(L_{2,3,4} - R\cos\theta_i) & \frac{2}{R^2\cos^2\theta_i}(2L_1 - R\cos\theta_i)(L_{2,3,4} - R\cos\theta_i) - 1 \end{bmatrix} \end{aligned} \tag{4}$$

Note that the following substitution was made: $L_{2,3,4} \equiv L_2 + L_3 + L_4$. In addition, the effective radius of curvature $R_e = R\cos\theta_i$ since in this co-planar model, all events occur in the plane of incidence.

3 Suppliers

After having found about the right RoC and AOI of the curved mirrors, I searched for mirror blanks that had the necessary specifications in the websites of the following suppliers: LaserOptik, FiveNine Optics, Perkins Precision Development, Coastline Optics, and ThorLabs. Since many did not seem to have exactly what we were looking for, I also directly contacted them individually to see if they could supply the right custom mirror blanks with appropriate coating. In particular, I asked, among other things, for RoCs of 89.84mm or 90.11mm and coatings that support 1550nm and 775nm or 1550nm and 387nm.

The requirement for the coating to support either of those sets of wavelengths is due to a need for cavity locking. This feedback process involves sending light that is an integer fraction of the main 1550nm light, which is the one meant to interact with the Rb atoms, in order to counteract disturbances in the length of the cavity, such as vibrations. Thus, support for 1550nm and 775nm (1550nm/2) or 1550nm and 387nm (1550nm/4) would allow us to maintain resonance on the principal 1550nm light through cavity locking. It is important to note, however, that 775nm light likely will not be viable given that it is too close to a Rb electron transition energy. Accordingly, as this supplier outreach remains ongoing, other integer-fraction wavelengths may end up being used.

4 Conclusion

The ultimate goal is to design an atomic cavity with a focused beam to achieve the sensitivity required for accurate detection. Future work will entail continuing to model the 3D, non-planar design that overcomes the limitations of planar cavities. Thus, key next steps primarily include advancing the design of non-planar cavities with the ray transfer matrices by implementing existing code to compute off-planar rotations (see Appendix B) and the off-diagonal matrices (after which the mirror placement and radius of curvature will be finalized), analyzing the system's robustness against potential errors such as placement and misalignment, and coordinating with suppliers for the production of the curved mirrors.

Acknowledgments

This work was supported by the National Science Foundation Research Experience for Undergraduates (NSF REU) program, the LIGO Laboratory Summer Undergraduate Research Fellowship program (NSF LIGO), the California Institute of Technology Student-Faculty Programs, and the Victor Neher SURF Fellowship. I would like to thank Torrey Cullen for providing the Finesse 3 code that I started with to model the cavity. I would also like to thank my co-mentors for their invaluable help and guidance throughout this project: Daniel Grass and Professor Lee McCuller.

References

[1] Sander M. Vermeulen, Torrey Cullem, Daniel Grass, Ian A. O. MacMillan, Alexander J. Ramirez, Jeffrey Wack, Vincent S. H. Lee, Kathryn M. Zurek, Chris Stoughton, and Lee McCuller. Photon Counting Interferometry to Detect Geontropic Space-Time Fluctuations with GQuEST. April 2024.

[2] Daniel A. Steck. *Classical and Modern Optics*. 2024. Originally published in 2006. Available online at `http://steck.us/teaching` (revision 1.8.5, 25 May 2024).

[3] Anthony E. Siegman. *Lasers*. University Science Books, 1986.

A Investigating Finesse 3's Definitions of w, w_0, z, and z_R.

The beam radius w, beam waist w_0, distance along optical axis z, and Rayleigh length z_R are all important parameters that characterize the Gaussian beam. Thus it was imperative to make sure that the way Finesse 3 defined these parameters agreed with how I was interpreting and using them in calculations. To this end, I used the following relations as described in [2]:

$$w_0 := \sqrt{\frac{\lambda z_0}{\pi}} \tag{5}$$

$$z_R = \frac{\pi w_0^2}{\lambda} \tag{6}$$

$$w(z) := w_0\sqrt{1 + (\frac{z}{z_R})^2} \tag{7}$$

I propagated a beam path and checked the parameter values it produced in Table (3). In particular, I used its value of w_0 at the main waist and its optical distance z (as seen under m2.p1.i) to calculate what z_R and w would be using Equations 6 and 7:

$$\begin{aligned} z_R(w_0 : 22.891\mu\text{m}, \lambda : 1550\text{nm}) &= 1.0621\text{mm} \\ w(z : 45.5\text{mm}) &= 980.95\text{mm} \end{aligned}$$

These values matched with those provided by Finesse 3, so I concluded that it uses the same definitions given by Equations 5, 6, and 7. However, this check also showed that Finesse 3 determines z to start at the beginning of the beam's path (i.e., $z = 0$ corresponds to M1), whereas the formulas define that at the beam waist (halfway between M1 and M2, or N.p1.i/N.p2.o)

Table 3: Table of beam properties at all optical elements along the beam trajectory. AOI = $3.2°$, $L_1 = 0.091$m, $L_2 = 0.42$m, $L_3 = 0.58$m, $L_4 = 0.42$m.

	z	w0	zr	w	RoC	S	Acc. Gouy	q
L0.p1.o	0 m	900.52 um	1.6436 m	914.52 um	-9.5746 m	-104.44 mD	0°	-0.291 + 1.644j
m3.p1.i	1 mm	900.52 um	1.6436 m	914.43 um	-9.6056 m	-104.11 mD	33.803m°	-0.290 + 1.644j
m3.p3.o	1 mm	900.52 um	1.6436 m	914.43 um	-9.6056 m	-104.11 mD	33.803m°	-0.290 + 1.644j
m4.p1.i	581 mm	900.52 um	1.6436 m	914.43 um	9.6056 m	104.11 mD	20.046°	0.290 + 1.644j
m4.p2.o	581 mm	900.52 um	1.6436 m	914.43 um	9.6056 m	104.11 mD	20.046°	0.290 + 1.644j
m1.p4.i	1.001 m	900.52 um	1.6436 m	980.95 um	4.515 m	221.49 mD	33.403°	0.710 + 1.644j
m1.p3.o	1.001 m	22.891 um	1.0621 mm	980.95 um	-45.525 mm	-21.966 D	33.403°	-0.045 + 0.001j
N.p1.i	1.0465 m	22.891 um	1.0621 mm	22.891 um	81.28 Gm	12.303 pD	122.07°	0.000 + 0.001j
N.p2.o	1.0465 m	22.891 um	1.0621 mm	22.891 um	81.28 Gm	12.303 pD	122.07°	0.000 + 0.001j
m2.p1.i	1.092 m	22.891 um	1.0621 mm	980.95 um	45.525 mm	21.966 D	210.73°	0.046 + 0.001j
m2.p2.o	1.092 m	900.52 um	1.6436 m	980.95 um	-4.515 m	-221.49 mD	210.73°	-0.710 + 1.644j
m3.p4.i	1.512 m	900.52 um	1.6436 m	914.43 um	-9.6056 m	-104.11 mD	224.09°	-0.290 + 1.644j

B Non-Planar Coordinate Rotations

In order to apply a rotation in the non-planar case, the following transformation is needed [3]:

$$\left[\begin{array}{c} x_2 \\ x_2' \\ \hline y_2 \\ y_2' \end{array}\right] = \left[\begin{array}{cc|cc} \cos\theta & 0 & \sin\theta & 0 \\ 0 & \cos\theta & 0 & \sin\theta \\ \hline -\sin\theta & 0 & \cos\theta & 0 \\ 0 & -\sin\theta & 0 & \cos\theta \end{array}\right] \left[\begin{array}{c} x_1 \\ x_1' \\ \hline y_1 \\ y_1' \end{array}\right] \equiv \left[\begin{array}{c|c} C_\theta & S_\theta \\ \hline -S_\theta & C_\theta \end{array}\right] \left[\begin{array}{c} x_1 \\ x_1' \\ \hline y_1 \\ y_1' \end{array}\right] \tag{8}$$

This will be necessary when determining the overall 4x4 matrix since the non-planar cavity involves rotating the coordinate axes several times. This would look like the following matrix product [3]:

$$\left[\begin{array}{c|c} C_\theta & -S_\theta \\ \hline S_\theta & C_\theta \end{array}\right] \times \left[\begin{array}{c|c} M_{xx} & 0 \\ \hline 0 & M_{yy} \end{array}\right] \times \left[\begin{array}{c|c} C_\theta & S_\theta \\ \hline -S_\theta & C_\theta \end{array}\right] = \left[\begin{array}{c|c} C_\theta^2 M_{xx} + S_\theta^2 M_{yy} & S_\theta C_\theta (M_{xx} - M_{yy}) \\ \hline S_\theta C_\theta (M_{xx} - M_{yy}) & S_\theta^2 M_{xx} + C_\theta^2 M_{yy} \end{array}\right] \tag{9}$$

Carrying these operations out in series for each optical element arranged in cascade will result in the overall 4x4 matrix. Thus, this procedure will be employed in order to determine the off-diagonal elements involving the rotations.